Article

Not peer-reviewed version

Structural Evolution of Olivine during Mechanochemically-Assisted Mineral Carbonation under CO2 Flow

Costantino Cau , Alessandro Taras , Laura Caggiu , Gabriele Masia , Stefano Enzo , Sebastiano Garroni , Fabrizio Murgia * , Gabriele Mulas *

Posted Date: 28 August 2024

doi: 10.20944/preprints202408.2027.v1

Keywords: CCUS; olivine; ball-milling; ex situ XRD; carbon mineralization

Article

Structural Evolution of Olivine during Mechanochemically-Assisted Mineral Carbonation under CO_2 Flow

Costantino Cau, Alessandro Taras, Gabriele Masia, Laura Caggiu, Stefano Enzo, Sebastiano Garroni, Fabrizio Murgia * and Gabriele Mulas *

Dipartimento di Scienze Chimiche, Fisiche, Matematiche e Naturali, Università degli Studi di Sassari, Via Vienna 2, 07100 Sassari (Italy)

* Correspondence: F.M. fmurgia@uniss.it; G.M. mulas@uniss.it

Abstract: The mechanism of the mechanically assisted mineral carbonation of commercial olivine under flow of CO_2/N_2 mixture has been elucidated by *ex situ* powder X-ray diffraction and Fourier-transform infrared spectroscopy. The overall CO_2 conversion depends to the rotation frequency of the mill's engine, and reached 85% within 90 minutes of mechanical treatment, at a flow rate of 2.5 l min^{-1}. By tuning the frequency rotation, the kinetics of CO_2 conversion changed from a sigmoid behaviour into a more complex reaction pathway, involving subsequent steps. The structural analyses suggest the clinochlore, a Mg- and Fe- containing aluminosilicate gathered among the components of olivine, is formed and consumed in different stages, thus promoting the CO_2 sequestration that eventually results into the formation of hydrated and anhydrous Mg-based carbonates.

Keywords: CCUS; olivine; ball-milling; ex situ XRD; carbon mineralization

1. Introduction

The unceasing production of anthropogenic CO_2 has been rising serious concerns among scientific community. Since the signing of Kyoto protocol, back in the 1997, tight policies have been implementing in order to decrease the amount of CO_2 generated from industrial processes and domestic activities, as well as to reduce the overall CO_2 concentration in the atmosphere, whose value above 420 ppm is targeted to play a role in global warming and climate change [1]. In this scenario, "carbon capture, utilisation and storage" (CCUS) encompasses the set of activities in the fields of basic science, technology development, regulatory affairs, etc., aimed at subtracting CO_2 from the atmosphere by permanent confinement, through the implementation of physical, chemical, biological CO_2 fixation/conversion, as well as developing processes with a zero net impact of CO_2, by directly capturing the CO_2 when it is produced [2,3]. Indeed, the release of CO_2 into the atmosphere primarily occurs from specific sources, including thermoelectric plants, foundries, cement factories, and so on. This category of CO_2, known as "capturable CO_2," is emitted near its production source, making it more manageable to trap using targeted technologies [4]. Among these, the post-combustion approach expected that the CO_2 is captured from the exhaust gases of the combustion process, and it is the most promising sequestration route as it comes just after the process that produces carbon dioxide [5,6]. The concentration of CO_2 in the exhaust gases is typically between 4-14 v/v%, with unfavourable conditions for gas separation at atmospheric pressure [7]. In these operating modes, the denitrified and desulphurised CO_2 reacts with liquid, such as MEA (methyl ethyl amine), the only widely used and established commercial solution, or filtered by specially designed membranes, rising concerns on the whole environmental sustainability of the process [8]. A more viable alternative to remove CO_2 being now on the spot is the so-called mineralization of carbon dioxide, *i.e.* its transformation into carbonates of alkaline and alkaline-earth metals starting from mafic and ultra-mafic minerals, as well as metal oxides or hydroxides. Among the minerals, olivine, serpentine,

 doi:10.20944/preprints202408.2027.v1

talc, basalt are some of the investigated minerals which gained wide attention due to low cost and large availability. In particular, olivine is an abundant mineral in the Earth's crust (>50% by upper mantle volume) commonly found in mafic igneous rocks [9]. The mineralisation process using Ca-Mg-Fe natural silicates was proposed in the pioneering reports of Seifritz [10] and Lackner [11] mimicking the phenomenon that naturally happens in the deep oceans. The whole set of reaction schemes accompanying CO_2 mineralization is quite complex and it is well known in the literature [8,12]. It is worth remembering that metal carbonate may be formed at expense of corresponding silicates or of other metal precursors, and these reactions can occur in parallel with metal oxidation, H_2 evolution and CO_2 reduction processes. However, the process occurs with too sluggish kinetics that limit its feasibility for large-scale purposes. Despite this main hurdle, several methods have been studied to increase the reaction rate of silicates in carbonation, such as chemical and electrochemical activation [13], thermal activation [12], the use of additives in the reaction fluid with high temperatures and pressures [14] or mechanochemical activation [14,15]. Thermal activation leads to dehydrating hydrosilicates, such as serpentine minerals but is ineffective on olivine [12]. Chemical activation allows for the removal of metal cations from silicates but involves a high additional cost for the disposal of hazardous acid sludge [16]. On the other hand, mechanical activation reduces the average size of the crystallites with a corresponding increase in the surface area and eventually in the active-reactive sites of the silicate. Even though this technique is energy-demanding, it could become effective if integrated with pre-existing processes [17]. In this regard, mechanical milling, with repeated fracturing on the reagent powders, would induce structural defects into materials, reduce the average size of mineral grains and expose new active surfaces in the reaction environment [18]. Mechanochemical treatment was found to be an effective way to enhance the reactivity of natural silicates [19,20] and several reports [9, 15,21,22] highlighted how the microstructural parameter and texture properties were influenced by type of grinding, duration, presence or liquid as water or ethanol. A further step forward was taken by highlighting that by grinding natural silicates (such as forsterite, serpentine and wollastonite) in the presence of CO_2 (reactive milling, RM) [23], promoted mechanochemical absorption of carbon dioxide in the form of metal carbonate. More recently, studies based on the mechanical treatment of olivine minerals conducted by our research group [24,25] have highlighted the effective CO_2 mechanosorption on silicates, although in batch conditions (under static CO_2 atmosphere). Nonetheless, there are no applications to processes mechanochemically activated and carried out in continuous-gas-feeding mode. This work aims at studying the behaviour of olivine as solid-state CO_2 store in flow conditions, driven by mechanochemical activation, thus simulating a mechanochemically induced process of post-combustion CO_2 capture and transformation, ideally applicable to an industrial process that continuously emits CO_2. Moreover, the conversion process will be investigated by a structural characterization to get more insight into the serpentinization process in dynamic conditions.

2. Materials and Methods

2.1. Synthesis

Commercial olivine was provided by SATEF (Norway) and it has employed for CO_2 conversion reaction without any further pre-treatment. The experimental setup, reported elsewhere [26,27], consisted of a prototype steel reactor for ball-milling, equipped with gas transfer lines, connected upstream to the CO_2 tank and downstream to a gas-chromatograph (GC). The GC was equipped with a GS-Q column and both hot wire and flame ionization detectors, HWD and FID, respectively, using He as carrier gas. The feed gas flow was regulated by mass flow controllers. Typically, 2 g of olivine and 0.3 mL of deionized water (silicate:H_20 = 6.67:1 weight ratio) were placed inside a stainless-steel mechanochemical reactor together with 3 spheres of 3.7 g each, made by the same material. The reactor (vessel), packaged in air, was inserted into the mixer clamp of a commercial Spex 8000 Mixer/Mill. The mill has been customized in order to tune the engine rotation frequency: in particular, 745, 875 and 1000 rpm have been selected for this work.

 doi:10.20944/preprints202408.2027.v1

2.2. Reactant Gas Mixture: Set-Up

The reactant gas mixture consisted of 10% CO_2 (purity = 99.995%), balanced in N_2. First, the reaction chamber was saturated by flowing 20 mL min^{-1} of the reagent gas mixture for 1 hour, to remove air. Subsequently, the feed gas flow was set to the nominal value of interest (typically 2.5 mL min^{-1}) before the reaction has started. In order to monitor the disappearance of CO_2 during the mechanically-activated process, its initial concentration was determined by averaging 10 samplings collected during 1 hour, that is considered as a blank. As a general procedure, the GC gas analyses of the reactant and product gaseous mixture were performed at selected times once the mechanochemical process started: the first gas sampling was carried out after 1 minute and the subsequent ones were collected at regular steps of 5 minutes for at least 3 hours of monitoring.

2.3. Percentage Conversion of CO_2

This parameter indicates the rate of CO2 transformed compared to that initially present

$$\%\ CO_2 conversion = \frac{[CO_2]_i - [CO_2]_{GC}}{[CO_2]_i} \cdot 100$$

where $[CO_2]_i$ and $[CO_2]_{GC}$ are the initial and measured CO_2 concentration expressed in v/v%, respectively.

Considering that the CO_2 concentration evaluated at the GC will be equal to

$$[CO_2] = fr \cdot\ CO_2\ Area$$

where *"fr"* is the response factor of the GC-column for CO_2 and *"CO_2 Area"* is the area of the integrated CO_2 signal in the chromatogram, the equation to calculate the CO_2 conversion rate can be rewritten as:

$$\%\ CO_2 conversion = \frac{CO_2\ Area_i - \ CO_2\ Area_{GC}}{CO_2\ Area_i} \cdot 100$$

The initial CO_2 concentration values were determined for each experiment as the average value of at least three coherent values.

2.4. Assessment of Phase Evolution during Reactive Milling

Structural characterization was performed on both pristine and reacted samples by powder X-ray diffraction (P-XRD). The analyses were performed using a Smart Lab (Rigaku) diffractometer equipped with a Cu rotating anode in a Bragg-Brentano geometry. The P-XRD patterns were collected setting a step size of 0.05° and a dwell time of 4 s per point. The identification of the crystallographic phases of the pristine olivine and of the formed products has been performed using the software Xpert Highscore; crystallographic index files (CIFs) were taken from the Crystallographic Open Database (COD) [28]. The relative abundance of the crystallographic phases in the samples, as well as their microstructural parameters, have been obtained by Rietveld refinement performed using the software MAUD [29]. In order to get more insights into the reacting mechanism of the CO_2 mineralization, *ex situ* P-XRD at selected milling time has also been performed and analysed according to the protocols afore described. To further corroborate the results of the P-XRD analyses, the evolution of the crystallographic phases as a function of the milling time has been flanked by infrared spectroscopy analyses. Spectra of the olivine samples were collected through a Fourier Transform FT-IR 480 Plus Spectrometer (Jasco) in the wavenumber region ranging from 4000 to 500 cm^{-1}. Microstructural characterization and elementary analysis on the olivine samples were performed by scanning electron microscopy (SEM), using a FEI Quanta 200 microscope, equipped with an energy dispersive X-ray spectroscopy (EDAX) detector.

3. Results and Discussion

Figure 1 showcases the P-XRD performed on the pristine olivine sample. From the profile matching and further Rietveld refinement, it arises that the commercial olivine is mainly constituted by a Mg-based nesosilicate with some Fe inclusion, namely forsterite (~92.5 wt.%), flanked by an inosilicate, ferrous enstatite (~5 wt.%) and clinochlore (~2.5 wt.%). The forsterite, crystallizing in an

 doi:10.20944/preprints202408.2027.v1

orthorhombic space group, *Pbnm*, features isolated SiO_4 tetrahedra pointing in opposite direction along the *c*-axis. The tetrahedra are only connected to MO_6 distorted ochtaedra by oxygen corner sharing. The central atom of these octahedra, which are usually labelled in literature as the M2 coordination sites, is the metallic bivalent cation, which could be both Mg^{2+} and Fe^{2+}. The other octahedral site for cation, namely M1, less distorted, connects two M2 octahedra along the *b*-axis, creating a tetrahedral interstitial site whose fourth face is shared with the SiO_4 tetrahedron.

Enstatite crystallizes in the orthorhombic *Pbca* space group, its structure showcases a series of edge-sharing SiO_4 tetrahedra which indefinitely creates chains along the *c*-axis. These chains are perpendicularly connected to the layers in which Mg^{2+} and Fe^{2+} randomly sits in both regular octahedral and distorted octahedral sites, whose coordination distance for the latter with the farthest O atoms exceed 2.5 Å.

Lastly, clinochlore crystallizes in a triclinic space group, $P\bar{1}$. Using *c*-axis as guide, its structure is constituted by two layers of isolated SIO_4 tetrahedra, oriented in opposite directions, which share three edge O atoms with an inner layer of octahedra, whose centre mainly hosts Al^{3+} atoms. Due to the strong Si-O bonds, these three layers are tightly bonded. The remaining O in each of the SiO_4 groups in both layers is shared with octahedra belonging to the so-called brucite layer [30], which is constituted by more distorted octahedra that host in their centres, Mg^{2+}, Fe^{2+} or Al^{3+} connected to O-H groups. The brucite layer is less tightly bonded to the three T-O-T group of layers previously described. Therefore, the overall hardness of the mineral is considerably lower than that of both forsterite and enstatite [31]. A more comprehensive structural description of the crystallographic phases found in the olivine is gathered in the Table 1, below.

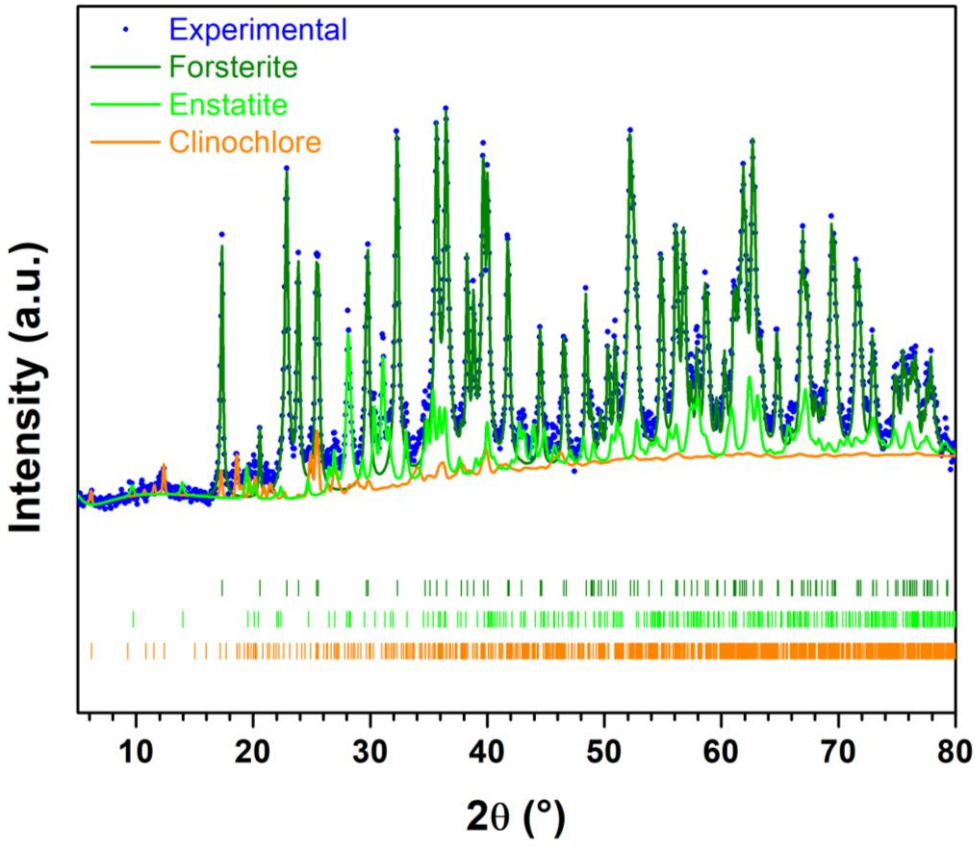

Preprints.org (www.preprints.org) | NOT PEER-REVIEWED | Posted: 28 August 2024 doi:10.20944/preprints202408.2027.v1

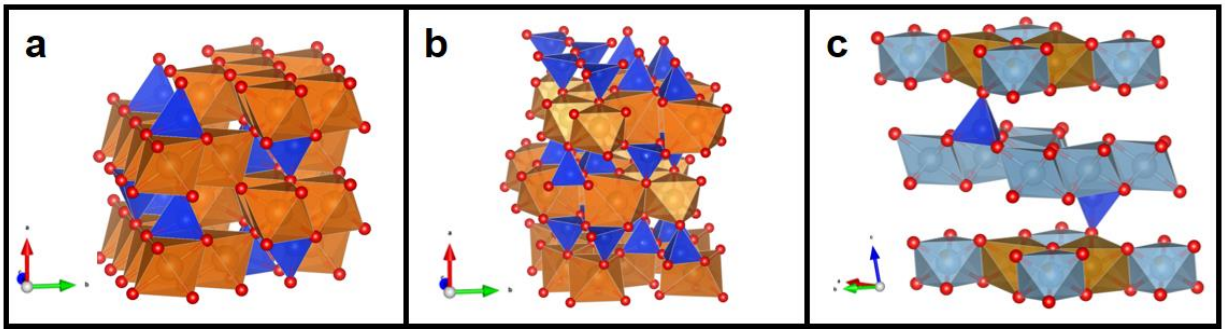

Figure 1. Top: P-XRD pattern of the pristine olivine. Rietveld refinement reveals that the main component is $Mg_{1.8}Fe_{0.2}SiO_4$, forsterite, ~92.5 wt.%, followed by $Mg_{0.8}Fe_{0.2}SiO_3$, ferrous enstatite, ~5 wt.% and $(Mg,Fe(II))_5Al(Si_3Al)O_{10}(OH)_8$, clinochlore, ~2.5 wt.%. Bottom: structural models of forsterite, enstatite and clinochlore, indicated by a, b and c, respectively.

Some morphology hints have been gained by SEM analyses: images presented in Figure 2 reveal that the olivine is constituted by a homogeneous distribution of millimetric and sub-millimetric particles with no regular shape. More interestingly, EDX analyses further confirm the presence of the typical elements that constitute the crystallographic phases listed above. In particular, Fe distribution fairly overlaps those of both Si and O, validating the presence of Fe in the main component of the olivine, *i.e.* the forsterite.

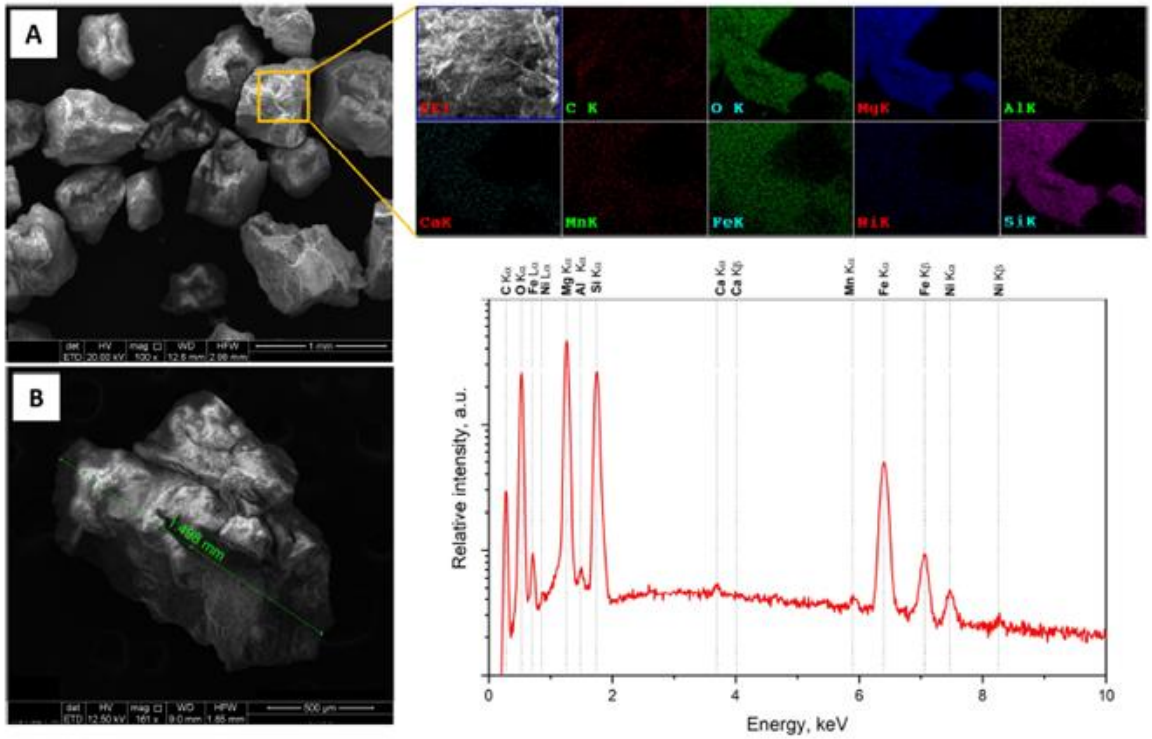

Figure 2. A: SEM micrography of pristine olivine particles, showing a narrow distribution of faceted micrometric particles (B: detail of a selected particle) and EDX analysis showcasing a homogeneous distribution of O, Mg, Si, Al and Fe, which are the main elements of the crystallographic phases composing olivine, flanked by some minor inclusions of Ca, Mn and Ni.

Figure 3 showcases the comparison of the CO_2 conversion kinetics over olivine treated at different rotation frequencies of mill engine. Regardless of the speed, is it noticeable the increase in the CO_2 conversion over time. The overall processes appear being not linear, albeit for the first 30 minutes of reactive milling a quasi-constant, steep increase in the conversion is visible. Indeed, after this period, a sudden change in the conversion behaviour is witnessed by the appearance of a plateau,

 doi:10.20944/preprints202408.2027.v1

which interestingly lasts longer as the rpm of the mill decreases. Subsequently, a new steep increase in conversion happens, followed by a second and eventually a third steady region that sets the maximum value of CO_2 conversion. In particular, the reaction carried out at 1000 rpm (red curve in Figure 3) reaches 85% of CO_2 conversion, which remains stable within the further monitored time interval.

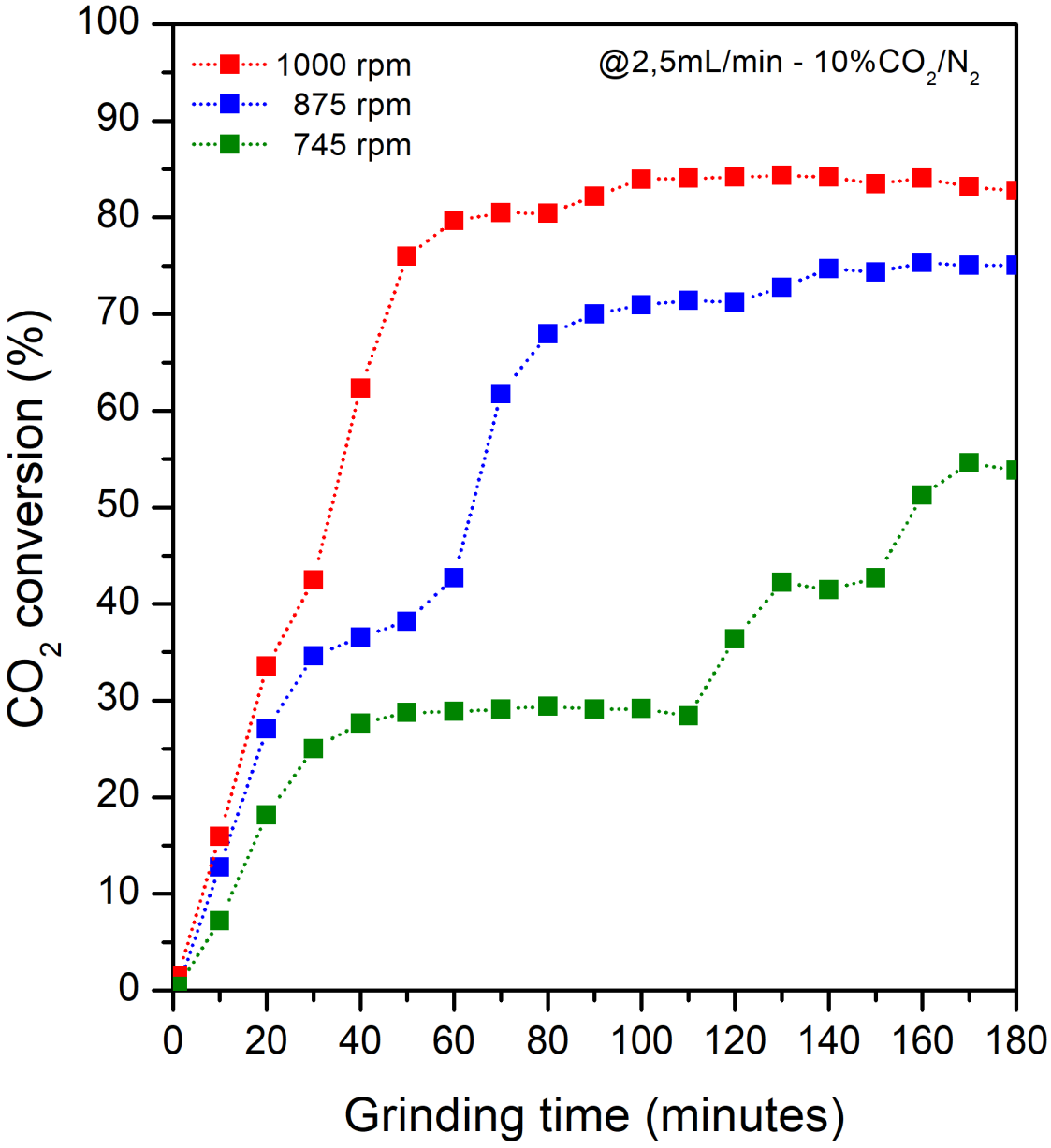

Figure 3. CO_2 conversion as a function of the grinding time; all the reported measurements are carried out by continuously flowing reacting gaseous mixture (2.5ml min^{-1}) into the jar. The rotation speed of the mixer/mill engine have been set at 745 (green scatters), 875 (blue scatters) and 1000 rpm (red scatters), which correspond to 12.4, 14.6 and 16.7 Hz, respectively. Dotted lines are added for the sake of clarity, and they should be intended only to help following the conversion trends at each of the rpm investigated. The conversion mechanism implies multiple stages, whose length depends on the rotation frequency, as witnessed by the different plateaus. The highest CO_2 conversion rate has been reached after 40 minutes of milling at 1000 rpm (red scatters, 85% of injected CO_2), being stable up to the end of the investigated time frame.

By varying the rpm of the mixer/mill engine, is it possible to tune the frequency of the impacts between the milling spheres and the reagents and eventually the mechanical energy transferred

 doi:10.20944/preprints202408.2027.v1

during each impact, per unit of time [32,33]. The variation of these two parameters occurs simultaneously with the increase in the rpm value and defines the intensity of mechanical treatment. The trends shown in Figure 3 comply with composite reaction mechanisms which are typical of solid-gas reactions involving several elementary steps, including CO_2 physical and chemical adsorption, diffusion, dissociation and conversion, and depend on the mechanical treatment conditions. More specifically, the reduction of the rotation frequency could unveil a multi-step process behind CO_2 conversion. Since the final conversion value within the observation time interval (180 minutes) increases with the rpm value, and the shape and extent of the intermediate plateau appear to be more pronounced as the rpm value decreases (particularly at 745 rpm, green curve in Figure 3), it is worth getting more insights into the reaction mechanism, by exploring the possible relations between crystallographic phase evolutions and kinetics of the solid-gas reaction.

Therefore, the phase evolution during the mechanical reaction carried out at 745 rpm has been followed by *ex situ* P-XRD at subsequent milling times, up to the end of the process, *i.e.* 180 minutes. The results, gathered in Figure 4, reveal the formation, yet at the earliest stages of milling, of hydrated and, subsequently, non-hydrated Mg-based carbonate phases, such as nesquehonite ($MgCO_3 \cdot 3H_2O$) and magnesite ($MgCO_3$), accompanied by variations of a few relative percentage points in the clinochlore. In particular, for milling times lying on the plateaus, the clinochlore slightly decreases, but is partly reformed at the end of each steep region (*i.e.* 140 and 180 minutes), whereas nesquehonite reaches its maximum during the first, longest plateau, reaching the value of almost 1 wt.% up to 60 minutes. The formation of these carbonates phases complies with the serpentinisation process [34] involving the oxidation of Fe^{2+} to Fe^{3+}. Nesquehonite could be formed yet at room temperature with a slight CO_2 overpressure and its conversion to magnesite occurs at a slightly higher temperature (around 90 °C) [35], which is a condition that can be locally achieved during a high-energy ball-milling. Indeed, mechanical milling has proven to be effective in various systems containing iron in order to trigger the reactivity, leading to solid solutions in binary systems, as well as to promote cationic substitution in ionic compounds [36,37]. Fe^{3+} can be included in a substitutional form in the sites of the Al^{3+} species in clinochlore, as reported in studies on the products of metamorphism of mafic rocks, which lead to the formation of minerals such as serpentinites and chlorites [38]. Likewise, as already observed in literature, the fixation of carbonate-based species is promoted by the basic environment arising from the minerals gathered in the olivine and is therefore responsible for the CO_2 chemical sequestration reported in Figure 3.

 doi:10.20944/preprints202408.2027.v1

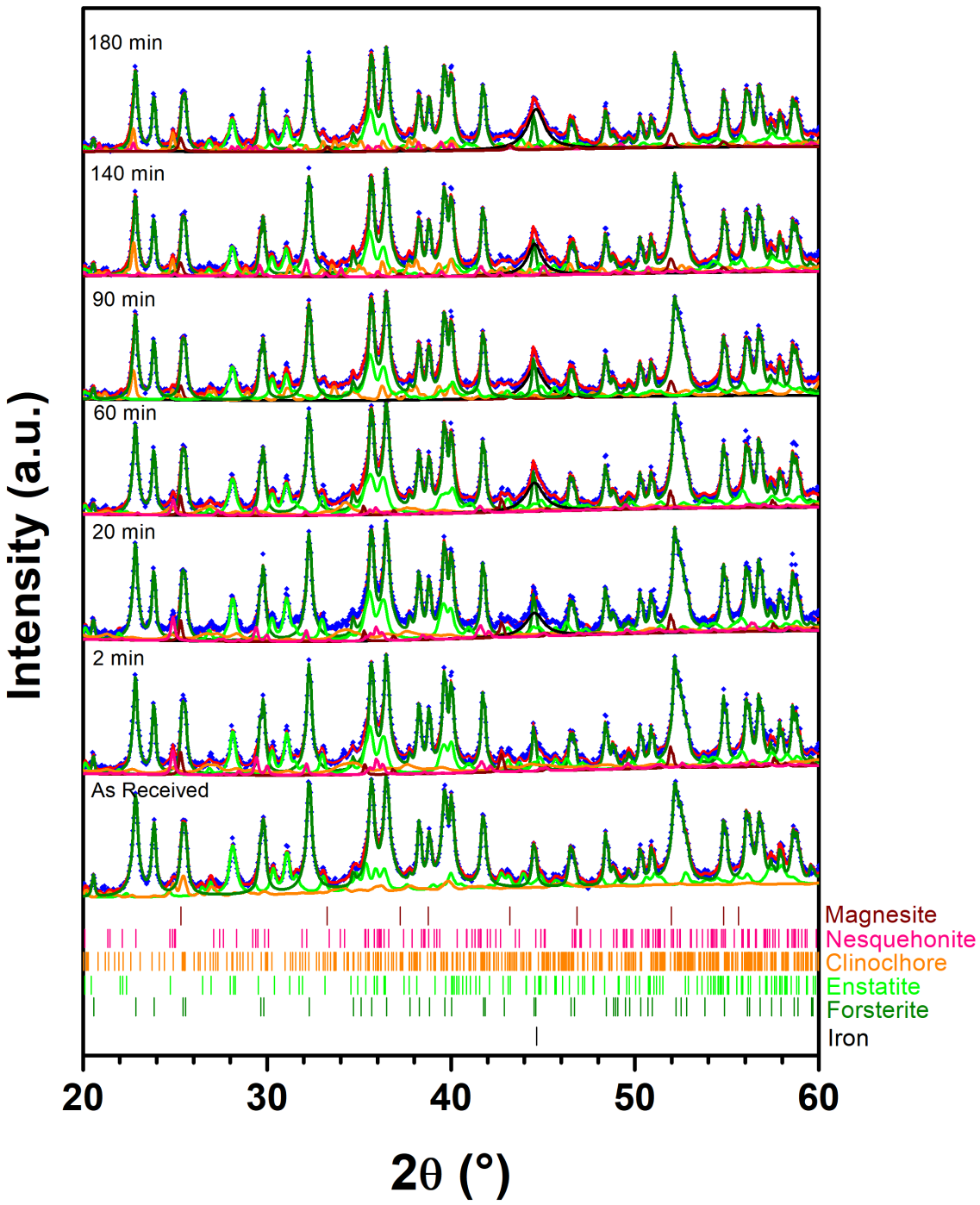

Figure 4. From bottom to top: structural evolution of the crystalline phases listed in the olivine sample at increasing milling times by ex situ P-XRD analyses, for the reaction carried out at 745 rpm and a constant flow, 2.5 l min^{-1}, of mixture gas containing 10% v/v CO_2. Stick patterns are added to better identify the contribution of every single crystallographic phase to each Bragg peak.

 doi:10.20944/preprints202408.2027.v1

Table 1. Cell parameters and relative abundancy and of the crystallographic phases obtained from Rietveld refinement on P-XRD patterns collected at subsequent milling stages, as well as the parameter Rwp%, which represents the weight ratio of the difference between the observation pattern and the XRD calculation.*[39]*.

↓ sample	Phase name →	forsterite ferroan	enstatite ferrous	clinochlore		nesquehonite		magnesite	iron
	formula →	$Mg_{1.8}Fe_{0.2}SiO_4$	$Mg_{0.8}Fe_{0.2}SiO_3$	$(Mg,Fe(II))_5Al(Si_3Al)O_{10}(OH)_8$		$MgCO_3{\cdot}3H_2O$		$MgCO_3$	α-Fe
	Sp. group →	*Pbnm*	*Pbca*	$P\bar{1}$		$P2_1c$		$R\bar{3}c$	$Im\bar{3}m$
pristine	*a* (Å)	4.76	18.26	5.15	α=93.95	–		–	–
	b (Å)	10.22	8.83	9.58	β=95.60	–		–	–
	c (Å)	5.99	5.20	14.42	γ=89.58	–		–	–
	Weight %	92.5	5.0	2.5		–		–	–
	Rwp %	11.43							
2 min BM	*a* (Å)	4.76	18.25	5.38	α=91.55	7.70		–	–
	b (Å)	10.22	8.83	9.52	β=102.24	5.37	β=89.99	–	–
	c (Å)	5.99	5.19	14.63	γ=88.67	12.11		–	–
	Weight %	91.0	4.4	3.4		1.1		–	–
	Rwp %	11.59							
20 min BM	*a* (Å)	4.76	18.26	5.40	α=92.21	7.70		5.03	
	b (Å)	10.22	8.83	9.52	β=101.71	5.38	β=90.01		
	c (Å)	5.99	5.19	14.61	γ=88.91	12.09		17.95	
	Weight %	91.1	5.2	2.9		0.4		0.2	0.2
	Rwp %	11.57							
60 min BM	*a* (Å)	4.76	18.26	5.32	α=93.24	7.71		5.05	2.86
	b (Å)	10.22	8.84	9.54	β=99.99	5.36	β=90.31		
	c (Å)	5.99	5.19	14.55	γ=91.47	12.10		17.85	
	Weight %	90.4	6.0	1.8		0.9		0.2	0.6
	Rwp %	11.34							
90 min BM	*a* (Å)	4.76	18.26	5.34	α=90.68	7.74		5.05	2.86
	b (Å)	10.22	8.84	9.39	β=98.11	5.36	β=90.71		
	c (Å)	5.99	5.19	14.47	γ=92.01	12.10		17.85	
	Weight %	90.6	6.5	1.8		0.3		0.2	0.6
	Rwp %	9.66							
140 min BM	*a* (Å)	4.76	18.26	5.42	α=91.67	7.73		5.43	2.87
	b (Å)	10.22	8.82	9.43	β=101.79	5.36	β=89.64		
	c (Å)	5.99	5.21	14.60	γ=88.37	12.02		16.62	
	Weight %	90.7	5.6	2.3		0.3		0.1	0.9
	Rwp %	11.90							
180 min BM	*a* (Å)	4.76	18.26	5.42	α=91.69	7.36		5.41	2.86
	b (Å)	10.22	8.82	9.42	β=101.75	5.52	β=90.78		
	c (Å)	5.99	5.25	14.60	γ=88.35	11.7		16.79	
	Weight %	88.8	6.3	2.4		0.4		0.2	1.8
	Rwp %	10.62							

The relative low percentages of carbonate-based phases, (less than or equal to 2 wt.%, fairly close to the quantification limit of Rietveld refinement) could be explained by both the dilution of the CO_2 in the feed mixture and by the mechanical stresses to which the new phases, forming at the surfaces of the particles, were subjected during the mechanical treatment. In some of the patterns, the phase identification procedure also allowed for the identification of α-Fe, whose source could be likely the

 doi:10.20944/preprints202408.2027.v1

contamination from the stainless-steel jar. The interpretation of the diffraction data of such a multiphase system characterised by a high number of Bragg reflections over the entire explored 2θ angular range is not straightforward, given that the precipitation of carbonates likely occurs at the surface of the particles and the further milling action hampers their continuous enlargement. Therefore, the validation of the proposed conversion mechanism also arises from FT-IR measurements carried out on the powders treated for different grinding times (Figure 5). Indeed, the first carbonate phase being found after just 2 minutes of reactive grinding is the nesquehonite, identified by the three characteristic bands whose wavenumbers can be found at approximately 1518, 1478 and 1430 cm^{-1}, respectively. These signals also persist in the ground sample for 20 and 60 minutes. Once the milling time overcomes 60 minutes, it is possible to notice the conversion from hydrated Mg carbonate to the related anhydrous magnesite ($MgCO_3$), whose presence can be witnessed until the end of the experimental observation. More in detail, the signals falling in that region correspond to the bond vibrations of CO_3^{2-} groups, as reported in literature [40]. Specifically, for the analysed samples, two characteristic bands are observed at 1423.9 and 1484.3 cm^{-1}, attributable to the stretching of the carbonate group of the magnesite, confirming the formation of the metallic carbonates as a consequence of the mechanical treatment. In addition, the signals at approximately 2500 cm^{-1} and 1680 cm^{-1} are attributable to the stretching of O-H groups and to the bending of H_2O, respectively. The continuous CO_2 reaction at the surface of the olivine further consumes H_2O, which is progressively removed from the environment of the reaction, thus also drained from the freshly formed nesquehonite [35].

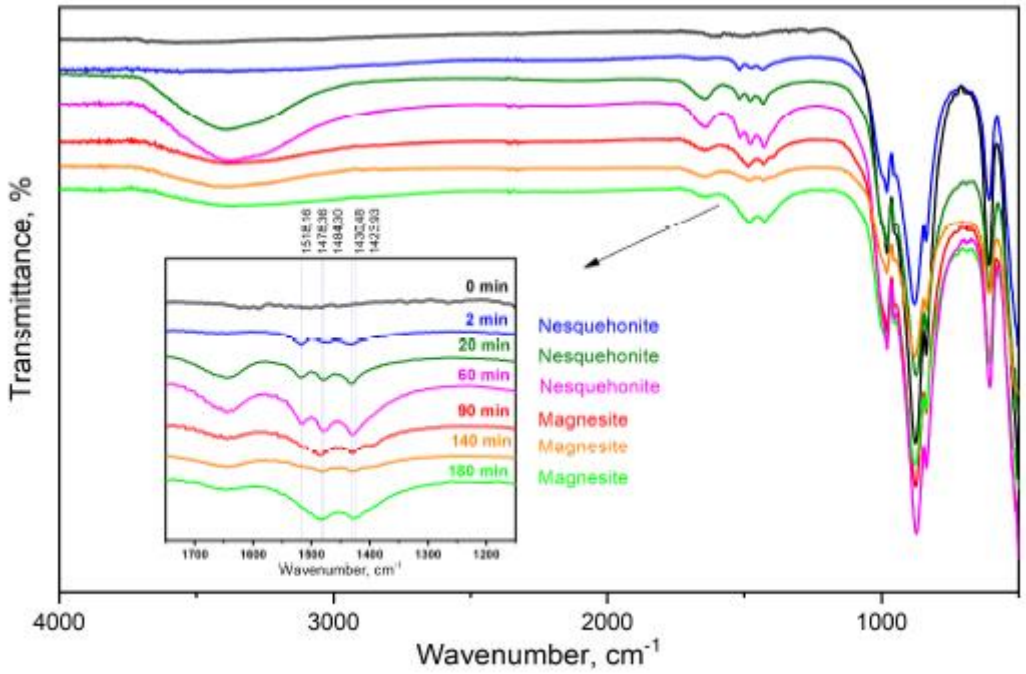

Figure 5. FT-IR analyses at different milling time further confirms the formation of hydrated Mg carbonate from the very early stages of reaction in CO_2 flow conditions (745 rpm, 10% v/v CO_2 concentration, 2.5 ml min^{-1}), thus followed by the appearance of signals that can be ascribed to the anhydrous magnesite (cf. Inset). Vibrations of the skeleton of the Si-O silicate matrix of olivine are also found, identifiable in the characteristic bands in the range 1000-500 cm^{-1}.

Lastly, in order to assess the possible direct effect of the high-energy grinding on the reactivity of the crystallographic phases that compose olivine, and eventually untangle it from the transformations due to the reactivity towards CO_2, a series of mechanical treatments have been performed at increasing milling time, from 1 to 10 hours on the olivine, without any further addition of reactive gas (Figure 6).

 doi:10.20944/preprints202408.2027.v1

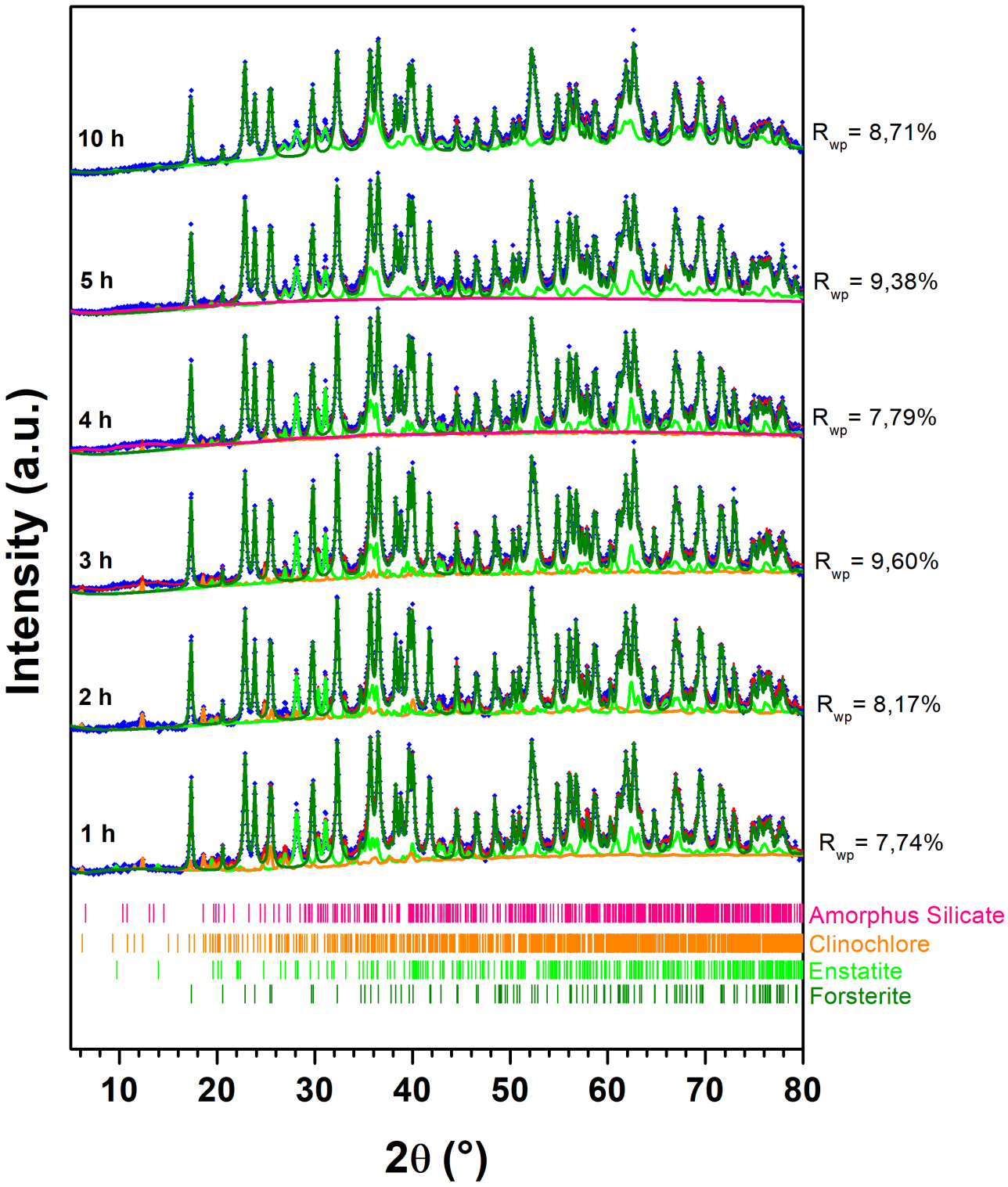

Figure 6. Left: XRD patterns (data points) and Rietveld refinement analyses (continue lines) of olivine mechanically treated material powders to mechanical grinding in a commercial Spex-type mill for times increasing from 1 to 10 hours, processing 8 g of powder per times with 2 spheres of 4 g each one, using a speed rotation of 750 RPM, in air atmosphere. Bar sequences of the peak positions expected from the geometry and lattice parameters of the considered phases (fingerprints) are reported at the bottom of the graph. The agreement factors (Rwp%) of the refinements are also shown, indicating the goodness of the data refinement procedure.

 doi:10.20944/preprints202408.2027.v1

From 1 to 3 hours of milling time, no qualitative difference can be observed with respect to the pristine sample: indeed, the three phases of olivine can be found, *i.e.* forsterite, enstatite and clinochlore. Nonetheless, slight changes in their relative abundance are noticeable from Rietveld refinement, due to the partial loss of crystallinity induced by the mechanical grinding (Table 2). For further milling time, from 3 to 10 hours, the contribution of the clinochlore phase to the pattern is lost. This could be due by a further amorphization that can be noticed in the amorphous shoulder at low scattering angles and eventually hides the presence of chlinoclore, although it is still visible after 3 hours of milling when CO_2 is flowed in the reactor. Moreover, also the Bragg reflections ascribed to the enstatite widen, whereas the signals belonging to the forsterite remain narrow, even up to 10 hours of mechanical grinding. Hence, the mechanical milling itself does not seem to play a crucial role either on enhancing the reactivity of olivine towards CO_2 by inducing any chemical transformation on the starting material, or by reducing the average crystallite size, since quasi-quantitative CO_2 conversion is reached before the effect of grinding on microstructure is even noticeable. More likely, high-energy ball-milling drives the CO_2 conversion by fracturing particles, thus exposing fresh surfaces in which solid-gas reaction can further take place. From the analyses of the gas chromatograph output data, the partial transformation of chlinoclore into magnesium carbonate triggered by CO_2 reduction reveals the release of hydrogen as well as light hydrocarbons, as could be expected by considering the results obtained in batch conditions. Nevertheless, some differences are noticeable and will be the object of further investigations by our research group.

 doi:10.20944/preprints202408.2027.v1

Table 2. Structural and microstructural data from Rietveld refinement on olivine as a function of the milling time. It is worth noting that by increasing the milling time, a partial amorphization on the sample occurs, therefore the overall weight % of the phases could not be 100. For the 5-h and 10-h samples, no clinochlore as crystalline phase was observable anymore.

↓ sample	Phase name →	forsterite ferroan	enstatite ferrous	clinochlore
	Chemical formula →	$Mg_{1.8}Fe_{0.2}SiO_4$	$Mg_{0.8}Fe_{0.2}SiO_3$	$(Mg,Fe(II))_5Al(Si_3Al)O_{10}(OH)_8$
	Space group →	*Pbnm*	*Pbca*	$P\bar{1}$
1h BM	*a* (Å)	4.76	18.25	5.15
	b (Å)	10.22	8.83	9.58
	c (Å)	5.99	5.20	14.42
	Grain size (nm)	105	54	123
	Weight %	93.7	4.0	2.3
	Rwp %	7.74		
2h BM	*a* (Å)	4.76	18.25	5.13
	b (Å)	1.23	8.83	9.55
	c (Å)	5.99	5.20	14.45
	Grain size (nm)	134	69	134
	Weight %	88.9	7.7	3.4
	Rwp %	8.17		
3h BM	*a* (Å)	4.76	18.26	5.11
	b (Å)	10.22	8.83	9.59
	c (Å)	5.99	5.20	14.47
	Grain size (nm)	124	78	121.15
	Weight %	88.8	8.3	1.7
	Rwp %	9.60		
4h BM	*a* (Å)	4.76	18.26	5.10
	b (Å)	10.22	8.83	9.59
	c (Å)	5.99	5.20	14.46
	Grain size (nm)	109	79	124
	Weight %	89.9	8.0	0.9
	Rwp %	7.79		
5h BM	*a* (Å)	4.76	18.26	-
	b (Å)	10.23	8.82	-
	c (Å)	6.00	5.20	-
	Grain size (nm)	88	29	-
	Weight %	88.7	10.3	Not found
	Rwp %	9.38		
10h BM	*a* (Å)	4.76	18.29	-
	b (Å)	10.23	8.78	-
	c (Å)	6.00	5.28	-
	Grain size (nm)	78	21	-
	Weight %	85.4	14.6	Not found
	Rwp %	8.71		

4. Conclusions

The kinetic profiles showcased by the reactions carried out at different rotation frequencies of the mill reveal that the CO_2 conversion process studied here cannot be described by a straightforward path of induction and subsequent fast growth, typically described by sigmoid functions. Indeed, by changing the rotation of frequency during the mechanochemically-driven CO_2 conversion, allowed us to unveil a more complex reaction mechanism that occurs through subsequent stages, whose

 doi:10.20944/preprints202408.2027.v1

features depend on the conditions of the mechanical treatment. The final conversion value within the observation time interval (180 minutes) increases with the rpm, while the shape and extent of the intermediate plateau appear to be more pronounced as the rpm decreases. This evolution suggests that the reaction speed of the CO_2 conversion lies on repeated formations and conversions of clinochlore, which acts as a trigger for the reaction that eventually lead to the precipitation of carbonate phases. Unless metallic cations (Mg^{2+} and Fe^{2+}) are available in all the phases listed in the studied olivine samples, the reason behind the particular reactivity of clinochlore might be found on its relative softness (2-3 in the Mohs scale of hardness) compared to those of both forsterite and enstatite (6-7). The repeated energy transfer due to the mechanical milling likely induces fractures in olivine where the softest component is present, thus exposing preferentially clinochlore to the incoming CO_2. Moreover, the magnesium carbonates, observed after the CO_2 conversion, arise from the Mg-containing brucite layers of clinochlore, the latter being loosely bonded to the aluminosilicate ones, therefore confirming the proposed topological description of the solid-gas reaction. Nonetheless, other studies are ongoing to correlate the kinetics of CO_2 sequestration with the distribution of gaseous products, with the aim to further shed light on the complex mechanism behind mineral carbonation under flow conditions.

5. Patents

- Method for Converting Crbon Dioxide into High Added Value Chemical Compounds through a Mechanochemical Process under Continuous Gas Flow Conditions Int. Patent WO/2022200941 A1 **2022**
- Process for the Conversion of Carbon Dioxide into Value-Added Products by Means of a Process of Mechanochemical Activation of Industrial Processing Scraps Int. Patent WO/2023199254 A9 **2023**

Author Contributions: Conceptualization, F.M., C.C., A.T. and G.M.; methodology, S.E., G.M.; software, F.M., L.C., S.E., S.G.; validation, S.E., S.G., F.M. and G.M.; formal analysis, A.T, C.C., F.M., L.C., S.E. and G.M.; investigation, C.C., A.T., G.Ma.; data curation, C.C., A.T.; writing—original draft preparation, A.T.; writing—review and editing, C.C., A.T., G.Ma., L.C., S.E., S.G., F.M. and G.M.; funding acquisition, S.G. and G.M. All authors have read and agreed to the published version of the manuscript.

Funding: The work has been funded by the resources of the "Fondazione di Sardegna" 2022 and 2023. This work has been also developed within the framework of the project e.INS- Ecosystem of Innovation for Next Generation Sardinia (cod. ECS 00000038) funded by the Italian Ministry for Research and Education (MUR) under the National Recovery and Resilience Plan (NRRP) - MISSION 4 COMPONENT 2, "From research to business" INVESTMENT 1.5, "Creation and strengthening of Ecosystems of innovation" and construction of "Territorial R&D Leaders".

Data Availability Statement: Data are available upon request to the Corresponding Authors.

Acknowledgments: The Authors deeply acknowledge Professor Radovan Černý for fruitful discussions.

Conflicts of Interest: The authors declare no conflicts of interest. The funders had no role in the design of the study; in the collection, analyses, or interpretation of data; in the writing of the manuscript; or in the decision to publish the results.

References

1. Busca, G. Critical Aspects of Energetic Transition Technologies and the Roles of Materials Chemistry and Engineering. *Energies* 2024, *17*, doi:10.3390/en17143565.
2. Zhang, Z.; Wang, T.; Blunt, M.J.; Anthony, E.J.; Park, A.H.A.; Hughes, R.W.; Webley, P.A.; Yan, J. Advances in Carbon Capture, Utilization and Storage. *Appl. Energy* 2020, *278*, 115627, doi:10.1016/j.apenergy.2020.115627.
3. Wei, R.; Alshahrani, T.; Chen, B.; Ibragimov, A.B.; Xu, H.; Gao, J. Advances in Porous Materials for Efficient Separation and Purification of Flue Gas. *Sep. Purif. Technol.* 2025, *352*, 128238, doi:10.1016/j.seppur.2024.128238.
4. Dubey, A.; Arora, A. Advancements in Carbon Capture Technologies: A Review. *J. Clean. Prod.* 2022, *373*, 133932, doi:10.1016/j.jclepro.2022.133932.

5. Liu, W.; Ji, Y.; Huang, Y.; Zhang, X.J.; Wang, T.; Fang, M.X.; Jiang, L. Adsorption-Based Post-Combustion Carbon Capture Assisted by Synergetic Heating and Cooling. *Renew. Sustain. Energy Rev.* 2024, *191*, doi:10.1016/j.rser.2023.114141.
6. Bukar, A.M.; Asif, M. Technology Readiness Level Assessment of Carbon Capture and Storage Technologies. *Renew. Sustain. Energy Rev.* 2024, *200*, 114578, doi:10.1016/j.rser.2024.114578.
7. Songolzadeh, M.; Soleimani, M.; Takht Ravanchi, M.; Songolzadeh, R. Carbon Dioxide Separation from Flue Gases: A Technological Review Emphasizing Reduction in Greenhouse Gas Emissions. *Sci. World J.* 2014, *2014*, doi:10.1155/2014/828131.
8. Dziejarski, B.; Krzyżyńska, R.; Andersson, K. Current Status of Carbon Capture, Utilization, and Storage Technologies in the Global Economy: A Survey of Technical Assessment. *Fuel* 2023, *342*, doi:10.1016/j.fuel.2023.127776.
9. Li, J.; Hitch, M. Structural and Chemical Changes in Mine Waste Mechanically-Activated in Various Milling Environments. *Powder Technol.* 2017, *308*, 13–19, doi:10.1016/j.powtec.2016.12.003.
10. Seifritz, W. CO2 Disposal by Means of Silicates. *Nature* 1990, *345*, 486.
11. Lackner, K.S.; Wendt, C.H.; Butt, D.P.; Joyce, E.L.; Sharp, D.H. Carbon Dioxide Disposal in Carbonate Minerals. *Energy* 1995, *20*, 1153–1170, doi:10.1016/0360-5442(95)00071-N.
12. McKelvy, M.J.; Chizmeshya, A.V.G.; Diefenbacher, J.; Béarat, H.; Wolf, G. Exploration of the Role of Heat Activation in Enhancing Serpentine Carbon Sequestration Reactions. *Environ. Sci. Technol.* 2004, *38*, 6897–6903, doi:10.1021/es049473m.
13. Vega, L.F.; Bahamon, D.; Alkhatib, I.I.I. Perspectives on Advancing Sustainable CO2 Conversion Processes: Trinomial Technology, Environment, and Economy. *ACS Sustain. Chem. Eng.* 2024, *12*, 5357–5382, doi:10.1021/acssuschemeng.3c07133.
14. O'Connor, W.K.; Dahlin, D.C.; Rush, G.E.; Dahlin, C.L.; Collins, W.K. Carbon Dioxide Sequestration by Direct Mineral Carbonation: Process Mineralogy of Feed and Products. *Miner. Metall. Process.* 2002, *19*, 95–101.
15. Haug, T.A.; Kleiv, R.A.; Munz, I.A. Investigating Dissolution of Mechanically Activated Olivine for Carbonation Purposes. *Appl. Geochemistry* 2010, *25*, 1547–1563, doi:10.1016/j.apgeochem.2010.08.005.
16. Azdarpour, A.; Asadullah, M.; Mohammadian, E.; Hamidi, H.; Junin, R.; Karaei, M.A. A Review on Carbon Dioxide Mineral Carbonation through PH-Swing Process. *Chem. Eng. J.* 2015, *279*, 615–630, doi:10.1016/j.cej.2015.05.064.
17. Li, J.; Hitch, M. Mechanical Activation of Magnesium Silicates for Mineral Carbonation, a Review. *Miner. Eng.* 2018, *128*, 69–83, doi:10.1016/j.mineng.2018.08.034.
18. Baláž, P.; Turianicová, E.; Fabián, M.; Kleiv, R.A.; Briančin, J.; Obut, A. Structural Changes in Olivine (Mg, Fe)2SiO4 Mechanically Activated in High-Energy Mills. *Int. J. Miner. Process.* 2008, *88*, 1–6, doi:10.1016/j.minpro.2008.04.001.
19. Zhang, Q.; Sugiyama, K.; Saito, F. Enhancement of Acid Extraction of Magnesium and Silicon from Serpentine by Mechanochemical Treatment. *Hydrometallurgy* 1997, *45*, 323–331, doi:10.1016/S0304-386X(96)00087-4.
20. Kalinkina, E. V.; Kalinkin, A.M.; Forsling, W.; Makarov, V.N. Sorption of Atmospheric Carbon Dioxide and Structural Changes of Ca and Mg Silicate Minerals during Grinding I. Diopside. *Int. J. Miner. Process.* 2001, *61*, 273–288, doi:10.1016/S0301-7516(00)00035-1.
21. Kalinkin, A.M.; Kalinkina, E. V.; Politov, A.A.; Makarov, V.N.; Boldyrev, V. V. Mechanochemical Interaction of Ca Silicate and Aluminosilicate Minerals with Carbon Dioxide. *J. Mater. Sci.* 2004, *39*, 5393–5398, doi:10.1023/B:JMSC.0000039252.13062.63.
22. Fabian, M.; Shopska, M.; Paneva, D.; Kadinov, G.; Kostova, N.; Turianicová, E.; Briančin, J.; Mitov, I.; Kleiv, R.A.; Baláž, P. The Influence of Attrition Milling on Carbon Dioxide Sequestration on Magnesium-Iron Silicate. *Miner. Eng.* 2010, *23*, 616–620, doi:10.1016/j.mineng.2010.02.006.
23. Bolm, C.; Hernández, J.G. Mechanochemistry of Gaseous Reactants. *Angew. Chemie - Int. Ed.* 2019, *58*, 3285–3299, doi:10.1002/anie.201810902.
24. Farina, V.; Gamba, N.S.; Gennari, F.; Garroni, S.; Torre, F.; Taras, A.; Enzo, S.; Mulas, G. CO2 Hydrogenation Induced by Mechanochemical Activation of Olivine With Water Under CO2 Atmosphere. *Front. Energy Res.* 2019, *7*, 1–10, doi:10.3389/fenrg.2019.00107.
25. Torre, F.; Farina, V.; Taras, A.; Pistidda, C.; Santoru, A.; Bednarcik, J.; Mulas, G.; Enzo, S.; Garroni, S. Room Temperature Hydrocarbon Generation in Olivine Powders: Effect of Mechanical Processing under CO2 Atmosphere. *Powder Technol.* 2020, *364*, 915–923, doi:10.1016/j.powtec.2019.10.080.
26. Taras, A.; Farina, V.; Cappai, L.; Enzo, S.; Garroni, S.; Mulas, G. Method for Converting Crbon Dioxide into High Added Value Chemical Compounds through a Mechanochemical Process under Continuous Gas Flow Conditions Int. Patent WO/2022200941 A1 2022.
27. Simula, M.D.; Taras, A.; Pinna L.; Piu S.; Enzo, S.; Garroni, S.; Mulas, G.. Process for the Conversion of Carbon Dioxide into Value-Added Products by Means of a Process of Mechanochemical Activation of Industrial Processing Scraps Int. Patent WO/2023199254 A9 2023.

28. Graulis, S.; Chateigner, D.; Downs, R.T.; Yokochi, A.F.T.; Quirós, M.; Lutterotti, L.; Manakova, E.; Butkus, J.; Moeck, P.; Le Bail, A. Crystallography Open Database - An Open-Access Collection of Crystal Structures. *J. Appl. Crystallogr.* 2009, *42*, 726–729, doi:10.1107/S0021889809016690.
29. Lutterotti, L. Total Pattern Fitting for the Combined Size-Strain-Stress-Texture Determination in Thin Film Diffraction. *Nucl. Instruments Methods Phys. Res. Sect. B Beam Interact. with Mater. Atoms* 2010, *268*, 334–340, doi:10.1016/j.nimb.2009.09.053.
30. Yang, M.; Ye, M.; Han, H.; Ren, G.; Han, L.; Zhang, Z. Near-Infrared Spectroscopic Study of Chlorite Minerals. *J. Spectrosc.* 2018, *2018*, doi:10.1155/2018/6958260.
31. Callister, William, D.; Rethwisch, D.G. *Materials Science and Engineering An Introduction*; Eight Edit.; Wiley, 2010; ISBN 0470419970.
32. Delogu, F.; Monagheddu, M.; Mulas, G.; Schiffini, L.; Cocco, G. Impact Characteristics and Mechanical Alloying Processes by Ball Milling: Experimental Evaluation and Modelling Outcomes. *Int. J. non-equilibrium Process.* 2000, *11*, 235–269.
33. Napolitano, E.; Mulas, G.; Enzo, S.; Delogu, F. Kinetics of Mechanically Induced Anatase-to-Rutile Phase Transformations under Inelastic Impact Conditions. *Acta Mater.* 2010, *58*, 3798–3804, doi:10.1016/j.actamat.2010.03.024.
34. Ugapeva, S.S.; Oleinikov, O.B.; Zayakina, N. V. Rare Hydrated Magnesium Carbonate Minerals Nesquehonite and Dypingite of the Obnazhennaya Kimberlite Pipe, in the Yakutian Kimberlite Province. *Minerals* 2023, *13*, doi:10.3390/min13111363.
35. Ballirano, P.; De Vito, C.; Mignardi, S.; Ferrini, V. Phase Transitions in the MgCO2H2O System and the Thermal Decomposition of Dypingite, Mg5(CO3)4(OH)25H2O: Implications for Geosequestration of Carbon Dioxide. *Chem. Geol.* 2013, *340*, 59–67, doi:10.1016/j.chemgeo.2012.12.005.
36. Enzo, S.; Mulas, G.; Frattini, R. The Structure of Mechanically Alloyed AlxFe(1-x) End-Products after Annealing. *Mater. Sci. Forum* 1998, *269–272*, 385–390, doi:10.4028/www.scientific.net/msf.269-272.385.
37. Farina, V.; Simula, M.D.; Taras, A.; Cappai, L.; Sougrati, M.T.; Mulas, G.; Garroni, S.; Enzo, S.; Stievano, L. Unveiling Redox Mechanism at the Iron Centers in the Mechanochemically Activated Conversion of CO2 in the Presence of Olivine. *J. Mater. Sci.* 2022, *57*, 10017–10027, doi:10.1007/s10853-022-06962-x.
38. Masci, L.; Dubacq, B.; Verlaguet, A.; Chopin, C.; Andrade, V. De; Herviou, C. A XANES and EPMA Study of Fe3+ in Chlorite: Importance of Oxychlorite and Implications for Cation Site Distribution and Thermobarometry. *Am. Mineral.* 2019, *104*, 403–417, doi:10.2138/am-2019-6766.
39. Toby, B.H. R Factors in Rietveld Analysis: How Good Is Good Enough? *Powder Diffr.* 2006, *21*, 67–70, doi:10.1154/1.2179804.
40. Turianicová, E.; Baláž, P.; Tuček, Ľ.; Zorkovská, A.; Zeleňák, V.; Németh, Z.; Šatka, A.; Kováč, J. A Comparison of the Reactivity of Activated and Non-Activated Olivine with CO2. *Int. J. Miner. Process.* 2013, *123*, 73–77, doi:10.1016/j.minpro.2013.05.006.